Indian Journal of Chemical Technology
Vol. 24, March 2017, pp.223-228

Synthesis of highly crystalline mesoporous TiO_2 by a fast sol-gel method

Qianqian Yin[1], Jingyu Xiang[1], Xiangdong Wang*[,1], Kui Zhang[1], Xiaoling Guo[2] & Guodong Shen[2]

[1]School of Science, Xi'an Jiaotong University, Xi'an 710049, China
[2]School of Textile and Materials, Xi'an Polytechnic University, Xi'an 710048, China
E-mail: wang90xd@163.com

Received 11 September 2015; accepted 2 July 2016

Mesoporous TiO_2 samples with high crystallinity have been successfully synthesized by a fast sol-gel method using polyethylene glycol (PEG) and polyacrylamide (PAM) as composite templates using two-step calcining processes. The samples have been characterized by X-ray diffraction, Transmission electron microscopy, N_2 adsorption-desorption and Diffuse reflectance UV-visible absorption spectra. The results show that the sample exhibits typical mesoporous structure and high crystallinity. The effects of PEG on properties of the samples and the effect of PAM on sol-gel reaction rate have also been studied. The results show that, PAM accelerates gel rate and PEG increased the crystallinity and specific surface area of the sample. Besides, visible light photocatalytic activity of mesoporous TiO_2 prepared by the fast sol-gel method is found to be improved.

Keywords: Mesoporous TiO_2, High crystallinity, Composite templates, Gel rate

In recent years, various mesoporous materials have been reported[1-3] since the discovery of mesoporous silica (e.g., SBA-15) in the 1990s[4]. Among the families, mesoporous TiO_2 materials have been synthesized via several approaches for immense potential applications in photocatalysis, sensors, and electrode materials because of its catalytic, optical, and electronic properties, especially in photocatalytic application[1,5-10]. Even though mesoporous TiO_2 is efficient in application of the UV light, its overall solar activity is very limited. Many studies suggest that the photocatalytic activity depends on the amount of electrons and holes on the surface of the photocatalyst in the reaction[11]. In addition, the small grain size leads to a shorter distance for the electrons and holes to transfer to the photocatalytic reaction sites, and many other factors, so efforts should be made to increase the specific surface area and decrease the grain size, thus improving photocatalytic activity.

Mesoporous TiO_2 in uniform size is synthesized by sol-gel method which is simple to handle, but the conventional sol-gel methods still have some disadvantages such as long preparation cycle, and mesoporous TiO_2 synthesized by this method has low thermostability and low crystallinity[12,13]. However, many applications can only be maximized in highly crystalline state. For example, when mesoporous TiO_2 is applied in photocatalysis, the amorphous regions are known to be trap sites for the recombination of photo-excited holes and electrons, limiting the efficiency of the device. High thermal and mechanical stability are also associated with the highly crystalline state[2,14-17]. Despite many efforts, up until today it remains a large challenge. To solve these problems, Lee *et al.* reported a new method in which an amphiphilic diblock copolymer, poly (isoprene-block-ethylene oxide), is used as the template to synthesize mesoporous TiO_2, which is calcined in Ar_2 atmosphere firstly and then recalcined in air atmosphere. The mesoporous TiO_2 prepared by this method not only has high crystallinity and thermostability but also has large surface area[8]. However, in this method, the cost of the template and argon is expensive, and the experimental procedure is tedious, limiting the application of the method.

In our previous work, we developed a fast sol-gel method to synthesis mesoporous TiO_2 with high specific surface area[18-20]. In this paper, we have used high molecular weight polyacrylamide (PAM) and polyethylene glycol (PEG) as composite templates, and used the method by means of an inorganic and organic molecular self-assamble reaction between the composite templates and tetrabutyl titanate. Then mesoporous TiO_2 with high crystallinity and large surface area were successfully synthesized by two-step calcination process. Finally, gel rate, crystallinity, crystallite size, pore size, specific surface area and photocatalytic activity of the samples were studied by X-ray diffraction (XRD), transmission electron microscopy (TEM), N_2 adsorption-desorption, and UV-Vis diffuse reflectance spectra. The photocatalytic activity of samples were studied by the photocatalytic degradation of methyl orange (MO) aqueous solution.

Experimental Section

Synthesis of the mesoporous TiO_2

A fast sol-gel preparation of the mesoporous TiO_2 was performed as follows. 10 mL deionized water and 6 mL nitric acid (5%) dissolved in 280 mL absolute ethanol were added in 10 mL tetrabutyl titanate. After the mixture was stirred at ambient temperature for about 1 h, the resultant solution was slowly added to the mixture of 0.2 g PAM (M_W = 3000000) and 0.8 g PEG (a series of M_W) dissolved in 30 mL of deionized water under vigorously stirring. A white gel was formed and dried at 60°C for 12 h. The obtained light yellow powder was calcined under N_2 atmosphere at 600°C, and then recalcined under air atmosphere at 500°C. As a comparision, the sample synthesized using 0.05 g of hexadecyl trimethyl ammonium bromide (CTAB) as a template and being calcined at 600/500°C in nitrogen/air was defined as t-TiO_2, in which the gel aged as long as 3 days.

Methods of measurement and characterization

XRD patterns of the photocatalysts were recorded at ambient temperature by a Bruker D8 Advance X-ray diffractometer (Cu Kα radiation, λ = 1.5406 Å) operated at 40 kV and 100 mA) and a 2 θ scan rate of 2º min^{-1}. The crystalline size was estimated by applying the Scherrer equation. N_2 adsorption-desorption isotherms were collected on an AUTOSORB-1 N_2 adsorption apparatus at -196°C and all samples were degassed at 120°C for 2 h. TEM was recorded on a JEM-2100F made in Japan. Diffuse reflectance UV-visible absorption spectra of the powder samples were obtained using a Shimadzu-2501 spectrophotometer. BaSO4 was the reference sample, and the spectra were recorded in the range of 200-900 nm.

Photocatalytic activity measurements

Photocatalytic degradation of MO was carried out in photocatalytic reactor. 10 mg/L of MO aqueous solution was prepared in advance, and 150 mg mesoporous TiO_2 samples were added into 60 mL of MO aqueous solution in 100 mL cylindrical vessel cooled by water-cycle condensing system. The mixture solution above was kept for 30 min in dark to reach adsorption equilibrium. Then it was stirred to make samples dispersed effectively by magnetic stirrer at the bottom of the reactor and was irradiated under visible light caused by a 300W xenon lamp located in the center of the cylindrical vessel at room temperature. About 4 mL the solution tooked out at regular intervals and was separated by a centrifugal machine. Then the supernate tooked out to be tested by spectrophotometer (UV-7220, Beifenruili, China) at 464 nm to determine relative absorbance to get the residual concentration of MO aqueous solution.

Results and Discussion

Synthesis mechanism

The mesoporous TiO_2 was prepared by next steps. Sol-gel method was conducted by using tetrabutyl titanate as the Ti source, and PAM and PEG as the composite templates. Firstly, PEG readily combined with the titania sol obtained from the hydrolyzation to form composite grains due to its strong hydrophilicity. These composite grains were incorporated with PAM by hydrogen bonding, and these grains were confined in the molecule network of PAM so that the process accelerates the sol-gel rate effectively. Then the above prepared precursor was successively calcined in a N_2 atmosphere and air atmosphere to remove the PEG and PAM. Finally, mesoporous TiO_2 with high crystallinity and specific surface area was obtained.

Influence of PAM

Figure 1 shows gel time varied for different concentrations of PAM. It can be seen that the gel time decreases sharply increase in the concentration of PAM. In the high concentration, gel had appeared even PAM had not been completely added. It's mainly based on two reasons: 1) Lone pair electrons on the nitrogen atom of the amide group and an oxygen atom form p-π-conjugated structure that reduces attraction of the nitrogen atom to the two hydrogen atoms near it, so the hydrogen atoms' chemical activity increases, which lead to the formation of hydrogen bonds of hydrogen atoms with

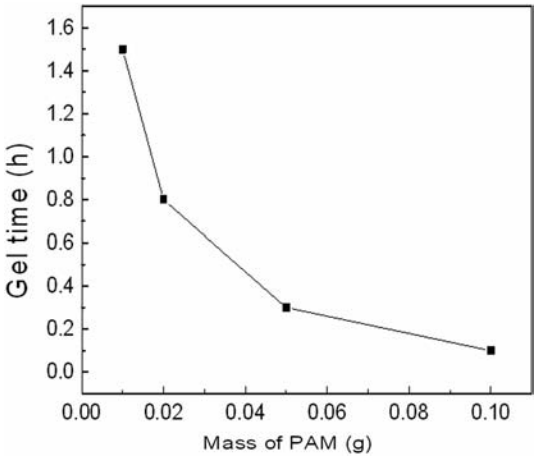

Fig. 1 — Gel time at different PAM concentration

other strong electronegative atoms. There were a large amount of hydroxyl groups on TiO_2 sol particle surface. In the solution system, TiO_2 sol combined with PAM by hydrogen bonds, that was the PAM surface covered with a layer of colloidal particles of TiO_2. PAM has played a similar role like colloidal nucleus which prevents TiO_2 colloidal particles to grow large. As a result, PAM limits the movement of TiO_2 colloidal particles so that it accelerates gel rate. 2) The PAM molecular chain contains a small amount of carboxyl groups and carboxylate ions which will generate ester groups by reacting with the hydroxyl groups on TiO_2 surface, that makes TiO_2 and PAM covalently combined. However, it worked not much obviously, which mainly because the carboxyl groups and carboxylate ions of PAM are limited[21,22]. Therefore, we can adjust the gel time by controlling the concentration of PAM.

Influence of PEG

Crystallinity

Figure 2 show the XRD patterns of the samples prepared using PEG of different molecular weights as template. The narrow diffraction peaks in the figure show the crystallinity of all the samples relatively high[23,24], especially for the sample prepared using of PEG (Mw=20000), which has the most narrow diffraction peaks. This is because when the sample was calcined at high temperature, the PEG will decompose and be carbonized to form amorphous carbon which will be filled in the sample and support around pore to prevent the mesostructure from collapsing due to rising temperature[25]. Thereby, PEG improves crystallinity of the sample without causing

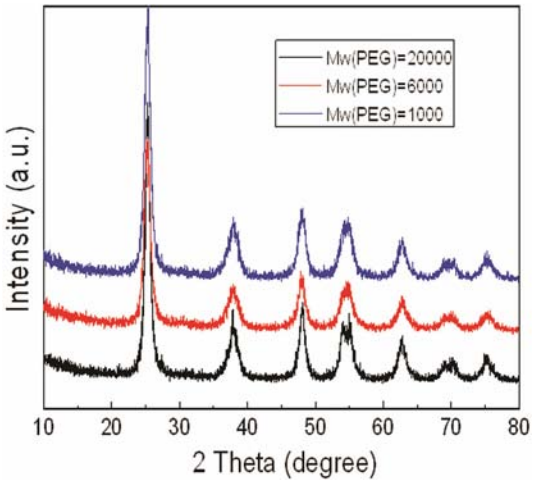

Fig. 2 — XRD patterns of mesoporous TiO_2 using PEG of different molecular weights

the specific surface area decreased rapidly.

Crystallite size

As shown in Table 1, the average crystallite sizes of the samples is about 7-11 nm, based on the XRD results calculating by Scherrer equation. The volume of PEG of different molecular weight affects crystallite size. For the PEG (Mw=20000), the crystallite size increases with increasing the volume of PEG. For PEG (Mw=1000), the crystallite size decreases with increasing the volume of PEG. For PEG (Mw=6000), the variation of crystallite size is irregular with increasing the volume of PEG. The reason of the results is that PEG lowers the critical micelle concentration (CMC) of colloidal particles. When the volume of PEG (Mw=20000) is 5 mL, the concentration of colloidal particles in solution is above CMC, the PEG will easily insert colloidal particles to increase the chance of collisions between colloidal particles, which increases the crystallite size of the sample. However, when the volume of PEG (Mw=1000) is 20 mL, the concentration of colloidal particles in solution has not reached the CMC, which was attributed to the molecular chains of PEG (Mw=1000) are so short that the effect of connecting colloidal particles is not obvious.

Specific surface area and pore size

Figure 3a shows nitrogen adsorption-desorption hysteresis loops for the samples using PEG of different molecular weights (the volume of all PEG in samples are 5mL). All adsorption isotherms are IV IUPAC classification and H_2 hysteresis loop. Hysteresis loops either appear in low pressure zone ($P/P_0<0.4$) or in high pressure zone ($P/P_0>0.8$), indicating that there exists either microporous structure or large particles' aggregating in the sample. There are obvious hysteresis loops in medium pressure zone ($0.8>P/P_0>0.4$), indicating that sample

Table 1 — Crystal structure parameters of mesoporous TiO_2 at different amount of PEG

Sample number	Molecular weight of PEG	V(PEG)/mL	Crystallite size/nm
1	—	0	19.79
2	20000	5	7.28
3	20000	15	9.64
4	20000	20	11.21
5	6000	5	10.38
6	6000	15	8.39
7	6000	20	9.75
8	1000	5	10.57
9	1000	15	8.37
10	1000	20	6.64

is very good in mesoporous structure.

Figure 3b and Table 2 show that the pore size of the sample remains at about 17.0 nm. The specific surface areas of all the samples shown in Table 2 are large and increase slightly with the different molecular weights. For PEG in tetrabutyl titanate-ethanol-water system, on the one hand, the ether bonds of PEG form hydrogen bonds with hydroxyls on the surface of TiO_2 to form a cladding layer on the surface of sample and prevent particles from aggregately growing, making a large amount of small clusters of TiO_2 generated in the solution, which are small in size and well-distributed, leading to the small sizes of samples[26]. On the other hand, when the calcination temperature in nitrogen atmosphere is up to 400°C, PEG will decompose and be carbonized to form amorphous carbon which will be filled in the sample and support around pore to prevent the mesostructure from collapsing due to rising temperature, leaving a large number of pores after the amorphous carbon is decomposed in air at higher temperature[27-30]. As a result, samples keep good mesostructure. The two mechanisms make the samples have large specific surface area. However, the specific surface area of samples varied not obviously with the different molecular weights, which may be because the crystallite size and the pore size of samples vary little for the PEG of different molecular weights.

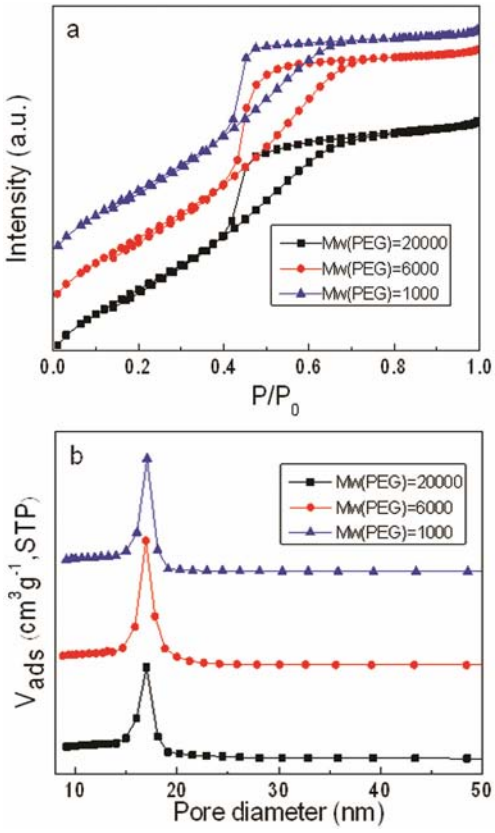

Fig. 3 — (a) N_2 adsorption-desorption hysteresis loops and (b) pore distribution of mesoporous TiO_2 using PEG of different molecular weights

Table 2 — Pore structure parameters of mesoporous TiO_2 using PEG of different molecular weights

Molecular weight of PEG	Specific surface area/m^2g^{-1}	Pore size/nm
20000	102.7	16.93
6000	104.2	16.92
1000	110.7	16.80

TEM analysis

Figure 4 shows that the TEM micrographs of the sample prepared at the calcination temperature of 600/500°C. It can be seen from Fig. 4a that the sample has a typical honeycomb porous structure with high crystallinity, in which the agglomeration of monodispersed TiO_2 particles is clear. It shows that the pore structures are like wormhole, being connected randomly and lacking discernible long-range order in the pore arrangement, and TiO_2 nanocrystals are embedded into the disorder mesoporous frameworks (Fig. 4b). As is seen in the Fig. 4c, the lattice fringe can be obviously measured in the HRTEM micrograph with an average interplanar space of 0.35 nm, which is similar to the sample from the corresponding wide-angle XRD pattern[22-24]. The pore size and particle size are respectively about 17 nm and 7-11 nm, which are in good agreement with the results of N_2 adsorption-desorption and XRD. The TEM image of selected area electron diffraction

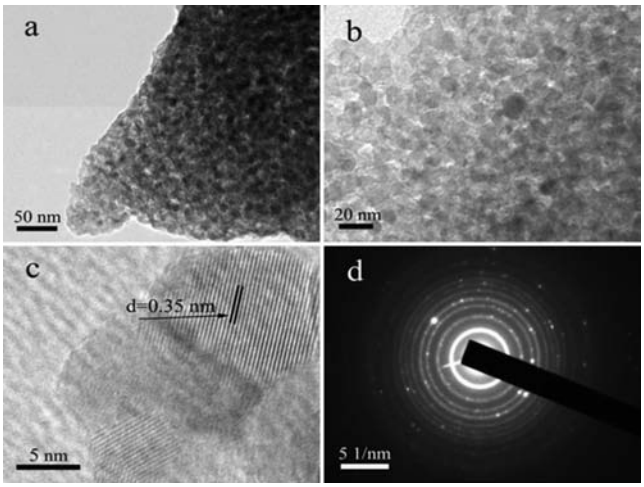

Fig. 4 — Samples characterized by TEM: (a) & (b) TEM images; (c) HRTEM image; (d) SAED pattern

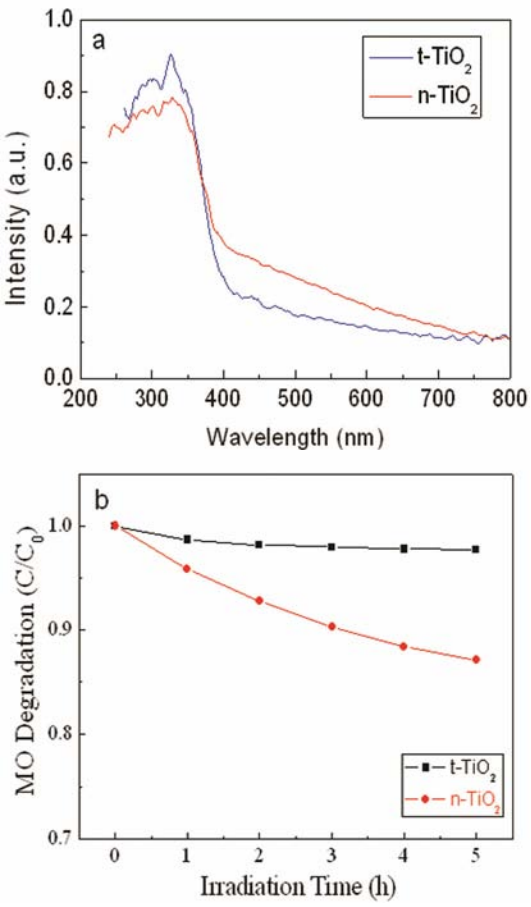

Fig.5 — (a) UV-Vis diffuse reflectance spectra and (b) photocatalytic activities of t-TiO_2 (by traditional method) and n-TiO_2 (by the method in this paper)

(SAED) pattern of the sample shows that a sequence of diffraction rings consistent with what is expected for the product as the crystal structure of the mesoporous material (Fig. 4d). Then the mesoporous TiO_2 with high crystalline and large specific surface area is obtained.

UV-Vis diffuse reflectance spectra

Figure 5a show the UV-Vis diffuse reflectance spectra of t-TiO_2 and n-TiO_2. As seen in the Fig. 5a, compared with t-TiO_2, the absorption intensity of n-TiO_2 is higher in the visible region and the n-TiO_2 exhibits a somewhat red-shift. The reason may be that the nitrogen element of PAM is partly doped into the TiO_2 lattice during calcination procedure. As a result, 2p orbital of nitrogen atom and 2p orbitals of oxygen atom overlap to form a new valence band and the valence band migrates towards conduction band which makes forbidden band wider[31]. As a result, the sample extends absorption into the visible-light region.

Photocatalytic activity

Figure 5b show the curves of MO degradation with time increasing driven by visible light to evaluate photocatalytic activities of t-$TiO_2$and n-TiO_2. It is obvious that the MO degradation of n-TiO_2 sample is more efficient. After 5 h of irradiation time, the degradation rates of n-TiO_2 and t-TiO_2 samples are about 23% and almost 3% respectively, indicating the higher photocatalytive activity of n-TiO_2 sample compared with t-TiO_2 sample. The visible photocatalytic activity of TiO_2 is depended on its absorption intensity of visible light. As shown in Fig. 5a, n-TiO_2 sample has higher absorption intensity of visible light than that of the t-TiO_2 sample, so n-TiO_2 sample exhibits a better performance in visible photocatalytic activity than t-TiO_2 sample.

Conclusion

The mesoporous TiO_2, with high crystalline and large surface area, was synthesized by using a fast sol-gel method, in which PAM and PEG were used as composite templates. PAM has played a similar role like colloidal nucleus, limiting the movement of TiO_2 colloidal particles, so it accelerated gel rate. When calcined in N_2 atmosphere, PEG was converted to a sturdy, amorphous carbon, which prevents mesostructure from collapsing when it is heated to the temperature required to get high crystallinity. PAM accelerated gel rate and PEG increased the crystallinity and specific surface area of the samples. Besides, compared with the mesoporous TiO_2 prepared by the traditional method, visible light photocatalytic activity of mesoporous TiO_2 prepared by the fast sol-gel method is improved.

Acknowledgements

This work was supported by the Natural Science Foundation of Shaanxi Province (2014JM-5057) and the Science and Technology Planning Project of Shaanxi Province (2013K09-04).

References

1 Navrotsky A, Trofymluk O & Levchenko A A, *Chem Rev*, 109 (2009) 3885.
2 Alibabaei L, Farnum B H, Kalanyan B, Brennaman M K, Losego M D, Parsons G N & Meyer T J, *Nano Lett*, 14 (2014) 3255.
3 Kresge C T, Leonowicz M E, Roth W J, Vartuli J C & Beck J S, *Nature*, 359 (1992) 710.
4 Zhao D, Feng J, Huo Q, Melosh N, Fredrickson G H, Chmelka B F & Stucky G D, *Sci*, 279 (1998) 548.

5 Robben L, Ismail A A, Lohmeier S J, Feldhoff A, Bahnemann D W & Buhl J-C, *Chem Mater*, 24 (2012) 1268.
6 Schüth F & Schmidt W, *Adv Mater,* 14 (2002) 629.
7 Wang X, Cao L, Chen D & Caruso R A, *ACS Appl Mater Interf*, 5 (2013) 9421.
8 Lee J, Orilall M C, Warren S C, Kamperman M, DiSalvo F J & Wiesner U, *Nat Mater*, 7 (2008) 222.
9 Kumar B V S, Sajan C P, Rai K M L & Byrappa K, *Indian J Chem Technol,* 17 (2010) 191.
10 Chen F, Li Y, Liu Z & Fang P, *Appl Surf Sci*, 341 (2015) 55.
11 Chen X, Liu L & Huang F Q, *Chem Soc Rev*, 44 (2015) 1861.
12 Hartmann P, Lee DK, Smarsly B M & Janek J, *ACS Nano,* 4 (2010) 3147.
13 Jaimy K B, Vidya K, Saraswathy HUN, Hebalkar N Y & Warrier K G K, *J Environ Chem Eng*, 3 (2014) 1277.
14 Atitar M F, Ismail A A, Al-Sayari S A, Bahnemann D, Afanasev D & Emeline A V, *Chem Eng J*, 264 (2015) 417.
15 Renuka N K, Praveen A K & Aravindakshan K K, *Mater Lett*, 91 (2013) 118.
16 Wang J, Li H, Li H, Zou C, Wang H & Li D, *ACS Appl Mater Interf*, 6 (2014) 1623.
17 Xie J, Bian L, Yao L, Hao Y & Wei Y, *Mater Lett*, 91(2013) 213.
18 Zhang K, Wang X, He T, Guo X & Feng Y, *Powder Technol,* 253 (2014) 608.
19 Xiang J, Yin Q, Zhang K, Guo X & Wang X, *Mater Technol,* 30 (2015) 213.
20 Zhang K, Wang X, Guo X, He T & Feng Y, *J Nanopart Res*, 16 (2014) 2246.
21 Sadeghalvaad M & Sabbaghi S, *Powder Technol*, 272 (2015) 113.
22 Tang Q, Lin J, Wu Z, Wu J, Huang M & Yang Y, *Eur Polym J*, 43 (2007) 2214.
23 Kim D S & Kwak S Y, *Appl Catal A-Gen,* 323 (2007) 110.
24 Moritz N, Areva S, Wolke J & Peltola T, *Biomater*, 26 (2005) 4460.
25 Sharma M K, Rohani P, Liu S, Kaus M & Swihart M T, *ACS Langmuir*, 31 (2015) 413.
26 Zhang Z, Yu F, Huang L, Jiatieli J, Li Y, Song L, Yu N & Dionysiou D, *J Hazard Mater*, 278 (2014) 152.
27 Liu E, Guo X, Qin L, Shen G & Wang X, *Chinese J Catal*, 33 (2012) 1665.
28 Jo E H, Chang H, Kim S K, Roh K M, Kim J & Jang H D, *Mater Lett*, 131 (2014) 244.
29 Naghibi S, Hosseini H R M, Faghihi Sani M A, Shokrgozar M A & Mehrjoo M, *Ceram Int*, 40 (2014) 5481.
30 Yang H, Zhu W, Sun S & Guo X, *RSC Adv,* 4 (2014) 32934.
31 Asahi R, Morikawa T, Ohwaki T, Aoki K & Taga Y, *Sci,* 293 (2001) 269.